

FULL PAPER

Open Access



# Tectonic effect for establishing a semi-dynamic datum in Southwest Taiwan

Kuo-En Ching<sup>1</sup> and Kwo-Hwa Chen<sup>2\*</sup>

## Abstract

To accommodate the effects of crustal deformation in the current national static geodetic datum (Taiwan Geodetic Datum 1997 (TWD97)) in SW Taiwan, 221 campaign-mode global positioning system (GPS) stations from 2002 to 2010 were used in this study to generate a surface horizontal velocity model for establishing a semi-dynamic datum in SW Taiwan. An interpolation method, Kriging, and a tectonic block model, DEFNODE, were used to construct the surface horizontal velocity model. Forty-four continuous GPS stations were used to examine the performance of the semi-dynamic datum through exterior validation. The average values of the residual errors obtained using the Kriging method for the north and east components are  $\pm 1.9$  and  $\pm 2.2$  mm/year, respectively, whereas those obtained using the block model are  $\pm 2.0$  and  $\pm 2.9$  mm/year, respectively. The distribution of residuals greater than 5 mm/year for both models generally corresponds to a high strain rate area derived using the horizontal velocity field. In addition, these residuals may result from deep-seated landslide and active folding or mud diapir in a mudstone area. Similar exterior checking results obtained using the Kriging interpolation method and block model for SW Taiwan indicate a high station density and a relatively satisfactory station spatial coverage. However, the block model is superior to the Kriging method due to the consideration of characteristics of the geological structure in the block model. In addition, result from traditional coordinate transformation was used to compare with the semi-dynamic datum. The results indicate that a semi-dynamic datum is a feasible solution for maintaining the accuracy of TWD97 at an appropriate level over time in Taiwan.

**Keywords:** GPS, Horizontal velocity model, Kriging interpolation, Block model, Coordinate transformation

## Background

Taiwan is located at the present-day plate convergence boundary between the Eurasian plate and the Philippine Sea plate (Fig. 1); earthquake activities are abundant and the convergence rate is approximately 82 mm/year across the island, reflecting a high surface strain rate of up to 1  $\mu$ strain/year (Yu et al. 1997; Bos et al. 2003; Chang et al. 2003; Byrne et al. 2011). However, the current Taiwan Geodetic Datum (Taiwan Geodetic Datum 1997 (TWD97)), announced in 2012, is considered a static geocentric datum, and it complied with the International Terrestrial Reference Frame 1994 (ITRF94) in the first epoch of 2010 (MOI 2012). The baseline accuracy in a horizontal component aimed at TWD97 is  $2.0 \text{ mm} + 1 \text{ ppm} \times k$ , where  $k$  is the length of the

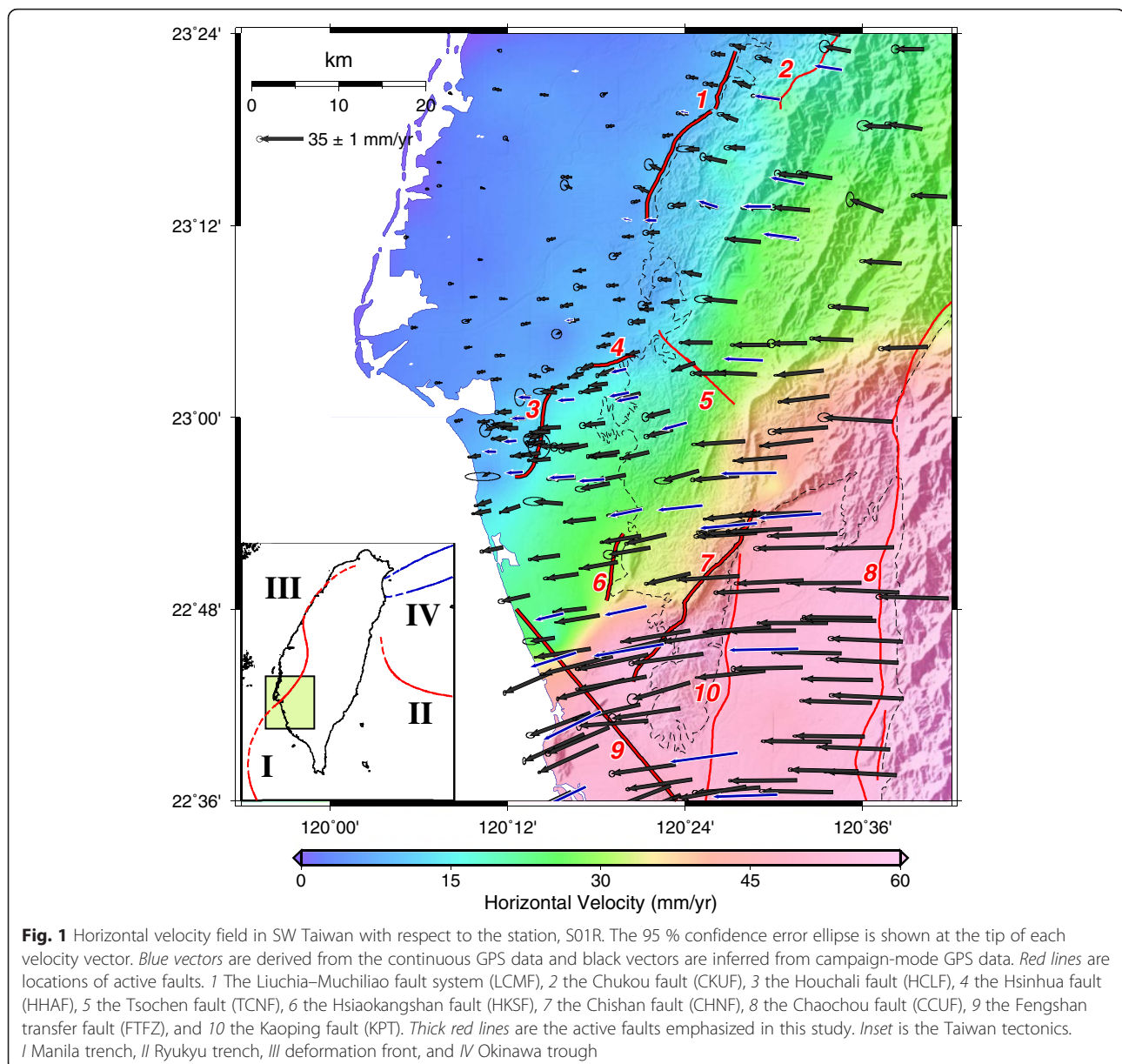
baseline, which corresponds to approximately 0.05 m horizontally. In other words, this datum will be distorted and lose its accuracy after 4–5 years because of the presence of a velocity gradient of up to 1  $\mu$ strain/year across the geodetic network. Therefore, the main concern in constructing a modern national geodetic datum in Taiwan is determining how to accommodate the effects of crustal deformation to maintain a spatial accuracy of its coordinates during a long period.

In general, establishing a semi-dynamic datum by assigning deformation models to a specific geodetic datum, such as the Japanese Geodetic Datum 2000 (Tanaka et al., 2007) and the New Zealand Geodetic Datum 2000 (Grant and Blick 1998; Beavan and Haines 2001; Beavan and Blick 2007), is an appropriate means for sustaining the coordinate spatial accuracy for a national-based geodetic datum at the plate boundary to account for the high surface strain

\* Correspondence: khchen@mail.ntpu.edu.tw

<sup>2</sup>Department of Real Estate and Built Environment, National Taipei University, New Taipei City 23741, Taiwan

Full list of author information is available at the end of the article



(Tregoning and Jackson 1999). The coordinate accuracy requirements have been achieved over time by using this deformation model. The long-term surface velocity resulting from interseismic plate tectonic loading and permanent surface displacement caused by discrete events, such as an earthquake, are generally included in the deformation model to reflect the true deformation field with adequate accuracy and resolution (Beavan and Blick 2007). Therefore, constructing a semi-dynamic datum is a solution for maintaining the accuracy of TWD97 at an appropriate level over time in Taiwan.

More than 750,000 people reside in SW Taiwan, and a high velocity gradient has been observed in this area

(Ching et al. 2007, 2011b) (Fig. 1). Previous studies have inferred a high contraction rate of approximately  $1.0 \mu\text{strain}/\text{year}$  with a clockwise rotation of  $14.5^\circ\text{--}27.1^\circ/\text{myr}$ , and right-lateral shearing from sparse global positioning system (GPS) horizontal velocities in the fold-and-thrust belt of SW Taiwan (Bos et al. 2003; Chang et al. 2003; Ching et al. 2007, 2011b; Hsu et al. 2009). In addition, the earthquake record from the Central Weather Bureau of Taiwan indicates that no  $M_L > 6.0$  earthquakes have occurred in our study area since 1900, except for the 2003  $M_w$  6.8 Chengkung earthquake in eastern Taiwan and the 2010  $M_w$  6.4 Jiasian earthquake occurred close to the study area. Most of the coseismic displacements

caused by those two earthquakes are smaller than 5 mm (e.g., Ching et al. 2011a). In other words, no major post-seismic deformation has disturbed the secular motion in this region. Consequently, SW Taiwan is an excellent area for establishing a semi-dynamic datum by estimating a horizontal velocity field to maintain the coordinate accuracy of sites.

The purpose of this paper is to provide a horizontal velocity model based on 265 GPS observations for estimating and predicting the coordinate changes associated with the horizontal crustal motion in SW Taiwan (Fig. 1). The interpolation method, the tectonic block model, and traditional coordinate transformation were used to analyze the accuracy in estimating and predicting the coordinate changes at arbitrary sites. This paper presents a comparison of efficiency between the interpolation method and block model.

### Geological background

The major geological characteristic in SW Taiwan is the thick Plio-Pleistocene mudstone, Gutingkeng Formation. The Gutingkeng Formation dominates the study area, and its presence is proposed to be responsible for the nonoccurrence of large earthquakes in SW Taiwan since the last century. The Gutingkeng Formation consists of gray sandy siltstone and sandy mudstone intercalated with lenticular greywacke and subgraywacke with abundant Mollusca (Chou 1971).

Six major active faults, the Liuchia–Muchiliao fault system (LCMF), the Hsinhua fault (HHAF), the Houchiali fault (HCLF), the Hsiaokangshan fault (HKSF), the Chishan fault (CHNF), and the Fengshan transfer fault zone (FTFZ) from north to south (Fig. 1), account for the surface motion observed in this study. For the LCMF (number 1 in Fig. 1), although this fault system has remarkable landscape feature based on studies of aerial photographs, the evidence of separation in strata is absent in the field (Sun 1971). The northern segment of the LCMF (the Muchiliao fault) is a blind thrust and might have reactivated during Late Quaternary (Shyu et al. 2005). The southern segment of the LCMF (the Liuchia fault) is also a thrust fault and cuts across Holocene sediments. For the HHAF (number 4 in Fig. 1), the length of unambiguous surface rupture associated with the 1946  $M_L$  6.3 Hsinhua earthquake is about 6 km (Bonilla 1977). The high dip angle of about 70° to 90° is deduced by the surface trenching data (Lee et al. 2000) and the focal mechanism solution of the 1946 Hsinhua earthquake (Cheng and Yeh 1989). For the HCLF (number 3 in Fig. 1), a normal fault associated with the growth of diapiric fold has first been proposed using the seismic gravity, drilling well and shallow seismic survey data (Hsieh 1972; Kuo et al. 1998). In addition, a reverse fault has also been proposed using the geophotograph technique (Sun 1964) and the repeated

geodetic survey and D-InSAR results (Fruneau et al. 2001; Huang et al. 2006, 2009; Mouthereau et al. 2002). For the HKSF (number 6 in Fig. 1), an obvious fault scarp indicates that the length of the NNE-striking HKSF is approximately 8 km and it dips to the east (Hsu and Chang 1979; Sun 1964). For the CHNF (number 7 in Fig. 1), the NE-trending CHNF is a reverse fault with left-lateral components according to slickenside analysis along the fault plane (Chen 2005). However, the fault analysis suggests a normal displacement on the CHNF (Gourley et al. 2012). In addition, GPS measurements indicate that the CHNF is a reverse fault with a right-lateral strike-slip component (Ching et al. 2007, 2011b; Hu et al., 2007; Lacombe et al., 2001). For the FTFZ (number 9 in Fig. 1), the N140°E-striking FTFZ has been detected by analyzing a geomorphic feature acquired from the Digital Elevation Model (DEM) (Deffontaines et al. 1994; 1997; Lacombe et al. 1999) and by conducting GPS surface velocity analysis (Ching et al. 2007).

### Methods

#### GPS data acquisition and processing

##### GPS data

GPS observations from 221 campaign-mode GPS stations used in this study were installed by the Central Geological Survey and 44 continuously operating GPS stations established by the Central Weather Bureau, the Academia Sinica, and the Central Geological Survey in the study area in SW Taiwan from 2002 to 2010 (Fig. 1). GPS surveys are generally conducted annually. A benchmark is usually occupied by more than two sessions per year. Each session is 6–14 h, and all available satellites are tracked and rising higher than a 15° elevation angle. The sampling interval for data logging is 15 s. The 44 continuous GPS stations are used for examining the accuracy of the horizontal velocity model established by the 221 campaign-mode GPS stations in the study area.

The campaign surveying and continuously recorded GPS data were processed session by session and date by date, respectively, by using Bernese software v.5.0 (Dach et al. 2007) to obtain precise station coordinates. Precise ephemerides provided by the International GNSS Service (IGS) were used and fixed during processing. Five global IGS fiducial stations surrounding Taiwan (IRKT, TSKB, GUAM, PERT, and IISC) on the International Terrestrial Reference Frame (ITRF2008) (Altamimi et al. 2011) were used to determine the coordinates of all campaign-mode and continuous GPS stations in the study area. The horizontal uncertainties of coordinates were estimated to be 2–5 mm.

#### Horizontal velocity field in SW Taiwan

The GPS horizontal velocities were estimated on the basis of the coordinate time series in a time span of

9 years from 2002 to 2010. The horizontal velocities for the east and north components were estimated using least squares estimation (LSE). An empirical equation  $y = a + bt + Hc$  for the study area was used to determine the standard deviation of the horizontal velocity field, where  $y$  is the coordinate in each component,  $a$  is the offset from origin,  $b$  is the velocity in each component,  $c$  is the coseismic offset of the 2003  $M_w$  6.8 Chengkung earthquake in eastern Taiwan and the 2010  $M_w$  6.4 Jiasian earthquake, and  $H$  is a step function (Fig. 2). The formal uncertainties

( $\sigma_{ls}$ ) obtained using the LSE of velocities were scaled by the amount  $k = (\text{mis}/2)^2$  (Ching et al. 2011b), where  $k$  is the effect of daily coordinate variation presented in the coordinate time series and  $\text{mis}$  is the residual of calculations and observations for the time series for the east and north components, respectively. The velocity uncertainty  $\sigma$  for each component was re-estimated using the equation  $\sigma = (\sigma_{ls}^2 \times k)^{1/2}$  (Ching et al. 2011b).

GPS horizontal velocities are relative to the station S01R at Penghu Island in the Chinese continental

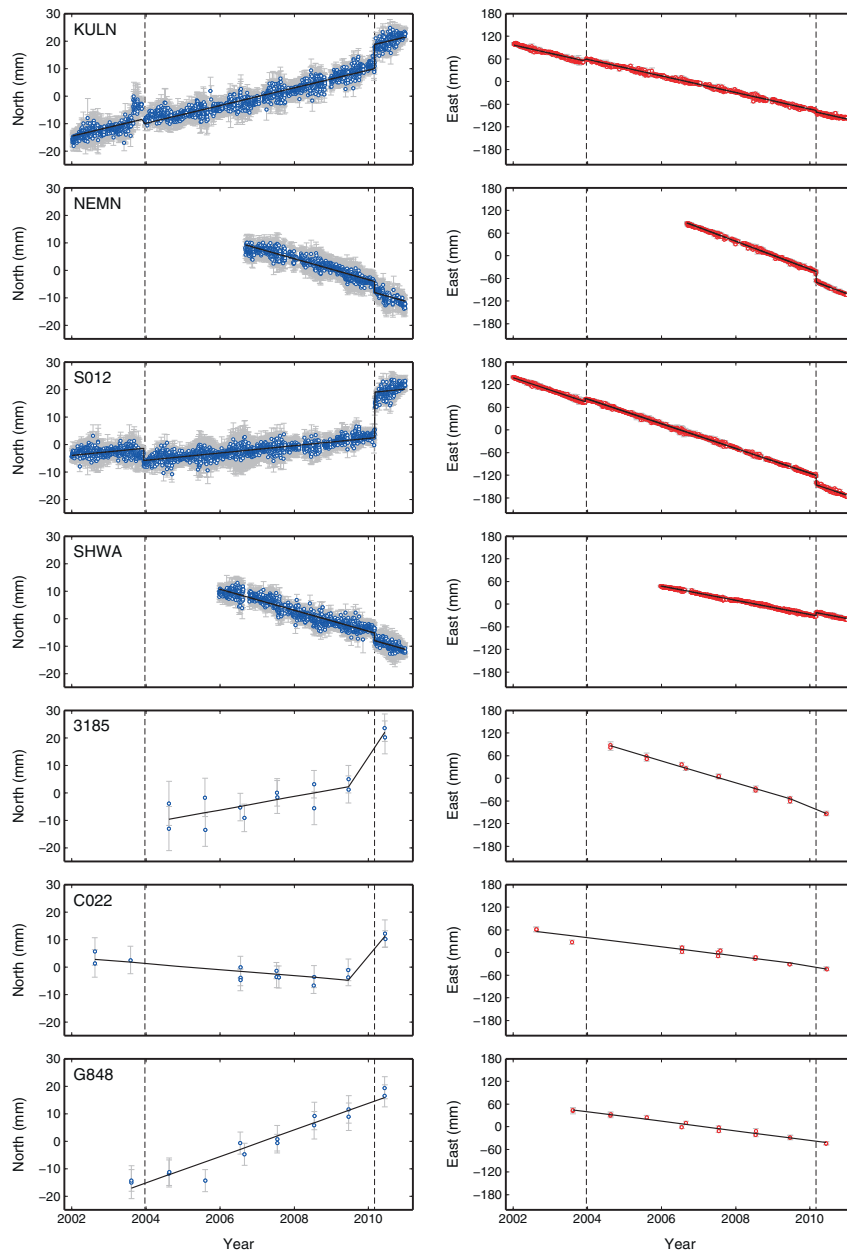


**Fig. 2** Selected coordinate time series. Blue and red circles are time series in north and east components, respectively. Black lines are data fitting. Two dashed lines are the epochs of the the 2003  $M_w$  6.8 Chengkung earthquake and the 2010  $M_w$  6.4 Jiasian earthquake

margin (Fig. 1). The horizontal velocities east of the CHNF are approximately 66 mm/year, N270°. The velocities gradually decrease westward to approximately 15 mm/year, N259°. The azimuths of velocities exhibit pseudo-counterclockwise rotation from EW to WSW. Most azimuths of velocities in the northern area are almost westward. However, the azimuths in the southern area rotate from nearly W (approximately 270°) to WSW (approximately 255°). A velocity gradient appears between the LCMF–HHAF–HCLF and the CHNF (Fig. 1).

### Establishment of surface velocity model

In this study, the interpolation method and tectonic block model were used to construct a surface horizontal velocity model. In general, the spatial variation of surface horizontal velocity is caused by the interaction between fault coupling and plate motion (e.g., McCaffrey 2002). A tectonic block which is a physical model containing the conservation of momentum and geological constraints (e.g., McCaffrey 2002) is therefore adopted in this study. On the other hand, a continuous surface velocity field is shown in our study area because most of active faults are locked at the surface. Hence, an interpolation method which is mathematical method is also properly adopted to obtain a surface velocity model in this area.

### Interpolation method

Various interpolation methodologies have been developed to construct new data points within the range of a discrete set of known data points using by curve fitting or regression analysis. Because the surface velocities containing a geographic feature are noisy data, a non-linear interpolation is needed not only for fitting an interpolant that passes through the given data points but also for regression. The Kriging interpolation which is mathematically closely related to regression analysis has been developed in geographic statistics for the estimation and prediction of spatial data (e.g., Roush et al. 2003; Samsonov and Tiampo 2006; van Dalen et al. 2006; Samsonov et al. 2007; Miura 2010; Majdański 2012). In the Kriging method, four frequently used semi-variance functions, exponential, Gaussian, linear, and spherical models, related

**Table 1** RMS analyses of the four semi-variance functions of Kriging interpolation method at 44 continuous GPS stations

	East component (mm/year)	North component (mm/year)
<sup>a</sup> Exponential	2.21	1.86
Gaussian	2.76	1.96
Linear	3.85	2.35
Spherical	2.22	1.89

<sup>a</sup>The optimal performance is obtained using the exponential model in this study

to the distances among sites can be employed to express the spatial variation, and they minimize the error of predicted values which are estimated by spatial distribution of the predicted values (Wackernagel 2003). Therefore, the Kriging interpolation is not dependent on given data points but on the data configuration and variogram parameters (Goovaerts 1997; van Dalen et al. 2006). Analyzing the root mean square (RMS; Eq. 1) of the differences between modeled and observed velocities at the 44 continuous GPS stations revealed that the optimal function is the exponential model. The results of RMS analyses for the four aforementioned semi-variance functions are shown in Table 1. The optimal performance relative to other functions is obtained using the exponential model (Eqs. 2 and 3).

$$\text{RMS} = \pm \sqrt{\frac{\sum_{i=1}^n (v_i^{\text{model}} - v_i^{\text{observed}})^2}{n}}, \quad (1)$$

where  $n$  is the number of sites and  $v_i^{\text{model}}$  and  $v_i^{\text{observed}}$  are the modeled and observed velocities at the 44 continuous GPS stations, respectively.

$$\gamma(h) = C_0 + C \cdot [1 - \exp(-h/a)], \quad \text{if } -h > 0 \quad (2)$$

$$\gamma(h) = 0, \quad \text{if } -h = 0 \quad (3)$$

where  $h$  is the lag distance between data point pairs,  $C_0$  is a nugget effect,  $C$  is a scale, and  $a$  is a range.

The horizontal velocities of the 221 campaign-mode GPS stations between 2002 and 2010 were employed with an assumption of equal weighting, and a horizontal velocity model with grids with 2.5-km spacing (approximately 90 s in both latitude and longitude) in the study area (70 km (E-W) and 80 km (N-S)) was generated using the Kriging method, and the exponential model with the range  $a = 15$  km (Eq. 2) due to the average of distances among the 221 campaign-mode GPS sites is approximately 5 km (Fig. 3). The critical semi-variance was set as  $C_0 + C$  (Eq. 2 if  $h \rightarrow \infty$ ) as the points were located at the exterior area of the observed sites, that is, 221 campaign-mode GPS stations. Moreover, to calculate the velocities at arbitrary points, the gridded velocities at the four points that form the cell in which the point lies were again interpolated using the bilinear method.

### Tectonic block model

The interseismic velocity field at the plate boundary zone is generally dominated by tectonic block rotations and interseismic coupling on faults (Savage and Simpson 1997). Based on this concept, an elastic kinematic block model with the code DEFNODE, developed by McCaffrey (2002), was adopted in this study to construct a surface horizontal velocity model for SW Taiwan. The nonlinear

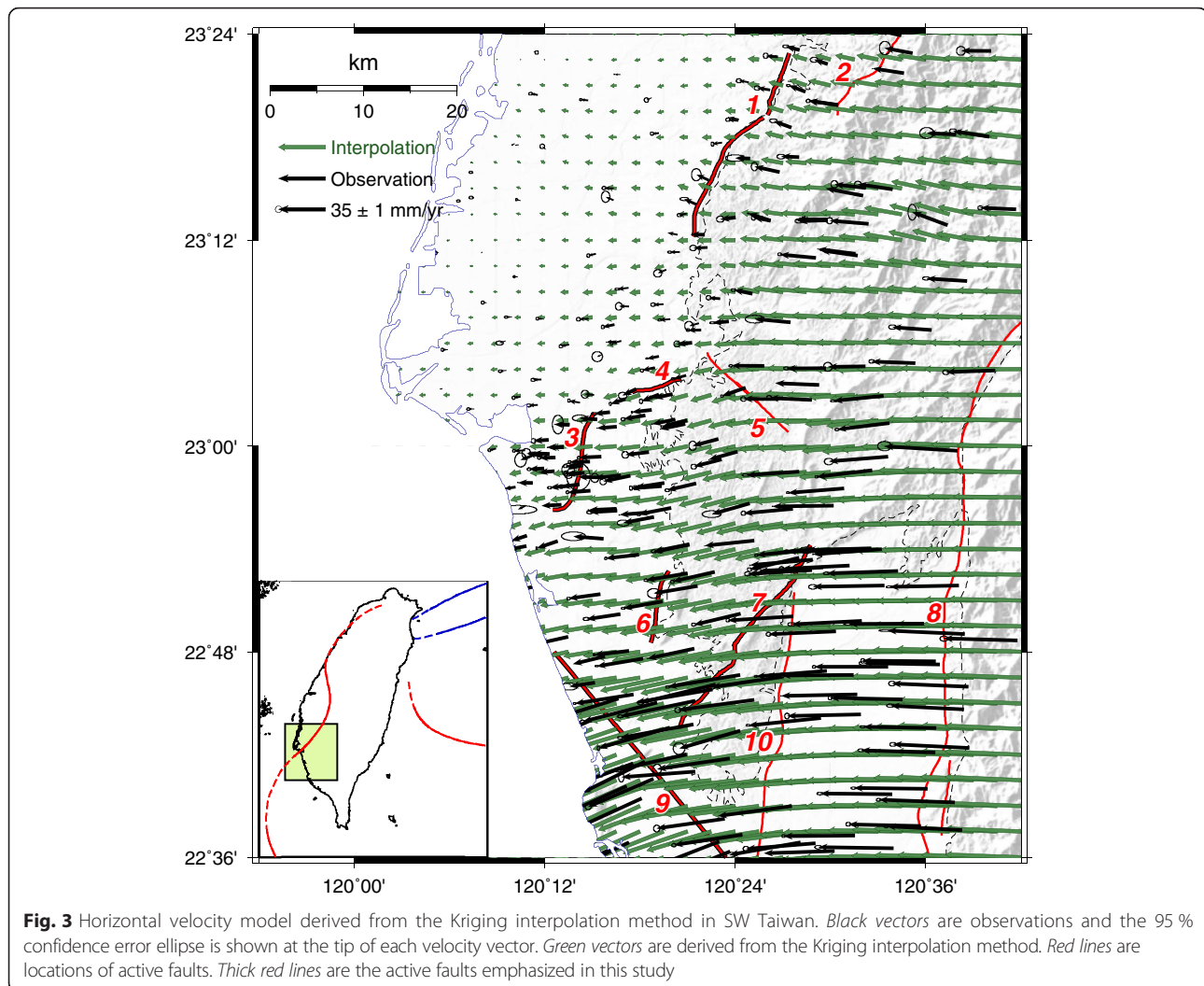


**Fig. 3** Horizontal velocity model derived from the Kriging interpolation method in SW Taiwan. *Black vectors* are observations and the 95 % confidence error ellipse is shown at the tip of each velocity vector. *Green vectors* are derived from the Kriging interpolation method. *Red lines* are locations of active faults. *Thick red lines* are the active faults emphasized in this study

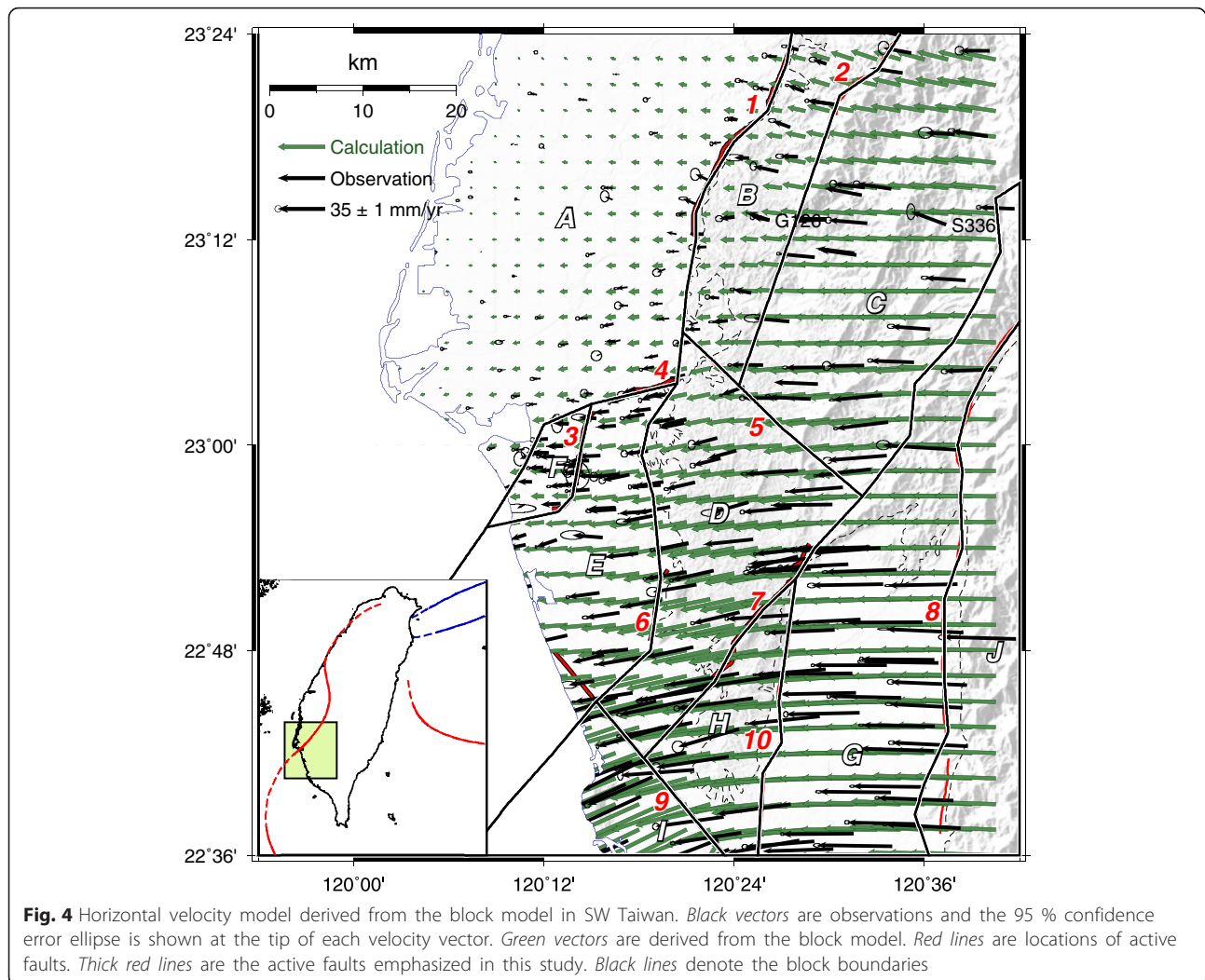
inversion in this program involved applying simulated annealing to downhill simplex minimization (Press et al. 1989) to invert GPS horizontal velocities simultaneously for Euler pole locations and the angular velocities of tectonic blocks and coupling coefficients on the block-bounding faults. The coupling coefficient is used to describe the velocity gradient, which is caused by the friction on the fault plane, across the fault. In this inversion, a constraint that decreases the coupling coefficient down-dip from being totally stuck at the surface to totally creeping at the bottom of the fault was imposed because most terrestrial faults in SW Taiwan exhibit no clear evidence of aseismic surface creeping. The contribution of fault coupling to the velocities was calculated using the formulations of Okada (1985) in an elastic half-space material. The best fit parameters were determined by minimizing data misfit, defined by the reduced chi-square statistic ( $\chi^2$ ) (McCaffrey 2002). A  $\chi^2$  value considerably greater than 1 indicates a relatively poor fit for the model, and a value close to 1 indicates an acceptable model fit.

### Tectonic blocks

Eleven elastic tectonic blocks in SW Taiwan were identified according to the concept proposed by Ching et al. (2011b) (Fig. 4). Because the trends of the GPS velocity gradients are generally parallel to the strikes of active faults in this region (red lines in Fig. 1), the block boundaries (black lines in Figs. 4 and 5) are mainly selected by determining whether the locations of GPS velocity gradients and active faults match. The blocks used in this study are closed, spherical polygons on the Earth's surface and cover the entire model domain. All points within a block are assumed to rotate with the same angular velocity.

### Fault configurations

The contribution of coupling on ten active faults to surface velocities in SW Taiwan was estimated according to the concept proposed by Ching et al. (2011b) in this study (Figs. 1 and 5). Faults with a slip rate are represented by a series of node points with 3-D shapes within



the spherical Earth (McCaffrey 2002) so that the fault dip and curvature are approximated. The fault geometries in the structural model, mainly modified by Ching et al. (2011b), are fixed in this model (Fig. 5). Faults are assumed to extend to a depth of 5–10 km, below which they creep at the full relative plate velocity. The exact dip angles for most reverse faults remain undetermined, and the lower edges of east-dipping thrusts in SW Taiwan increase from west to east with a depth from 5 to 7 km and with dip angles from approximately 25° to approximately 45°. In addition, because the depths and dip angles of two nearly E-W-striking strike-slip faults are still unclear, the fault depths of the Hsinhua (number 4 in Fig. 1) and Fengshan transfer faults (number 9 in Fig. 1) were set as 10 km, and the nearly vertical fault planes (dip angles between 90° and 70°) were assigned on the basis of limited balanced cross sections (Huang et al. 2004).

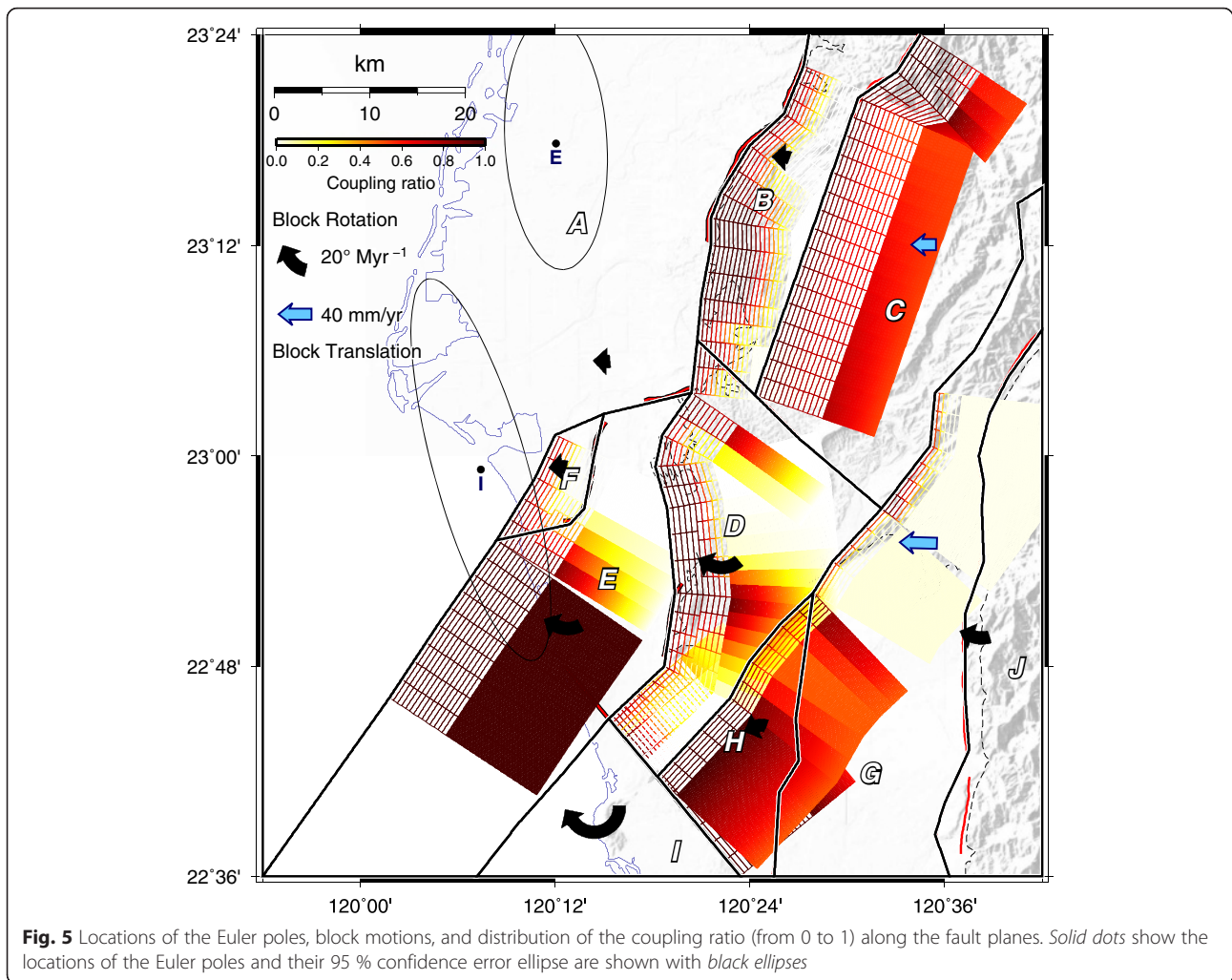
## Results and discussion

### Kriging method interpolating results

The  $RMS^{interior}$ , denoting the residual errors of the horizontal velocities of the 221 campaign-mode GPS stations, was evaluated using Eq. 1. The average  $RMS^{interior}$  is  $\pm 0.3$  mm/year for both north and east components (Fig. 6a). Model residuals are generally lower than  $\pm 2.0$  mm/year (Fig. 6a). However, the residual for the CHNF area is greater than  $\pm 3.0$ – $4.0$  mm/year (number 7 in Figs. 1 and 6a).

### Tectonic block modeling results

The preliminary locations of Euler poles for each tectonic block were calculated by inverting horizontal velocities without considering the effect of elastic strain because of the locking on the faults. The locations of Euler poles and the angular velocities of the aforementioned inversions serve as a priori information in inversions for motions of tectonic blocks and interseismic coupling on faults (Fig. 5).



The reduced  $\chi^2$  statistic of the optimized model is 1.29. Model residuals are generally lower than 2.0 mm/year (Fig. 6b). However, the residual around the CHNF region is greater than 4.0 mm/year (number 7 in Figs. 1 and 6b). The  $\text{RMS}^{\text{interior}}$  residual errors of the 221 campaign-mode GPS stations are  $\pm 2.8$  and  $\pm 2.0$  mm/year for the east and north components, respectively.

#### Coordinate transformation

Conventionally, the two-dimensional coordinate transformations are used to transform the coordinates of stations from the observed time  $t_0$  to a specific epoch  $t_1$  by applying a four-parameter transformation (Helmert transformation) (Ghilani 2010) or six-parameter transformation (affine transformation) (Chang 2004) to reduce the horizontal distortions caused by the crustal deformation in a local area. The six-parameter transformation is more commonly used than the four-parameter transformation because it uses more geometric parameters to absorb the horizontal deformation. Therefore, six-parameter transformation was adopted in this study.

The six-parameter transformation (Eqs. 4 and 5) uses 33 control points (Fig. 6a), which were selected from the 221 campaign-mode GPS stations in the study area (Fig. 1) by using the LSE method.

$$x' = ax + by + f \quad (4)$$

$$y' = cx + dy + g, \quad (5)$$

where  $(x, y)$  and  $(x', y')$  are the coordinates of the control points in the epochs  $t_0$  and  $t_1$ , respectively, and  $a, b, c, d, f,$  and  $g$  are the six parameters of the coordinate transformation.

To avoid the contamination of coseismic displacements resulting from the 2003  $M_w$  6.8 Chengkung earthquake and the 2010  $M_w$  6.4 Jiasian earthquake, the period adopted for the coordinate transformation experiment was 2004–2009. Therefore, the six parameters were evaluated for five periods, 2004–2005, 2004–2006, 2004–2007, 2004–2008, and 2004–2009, by using the LSE method.



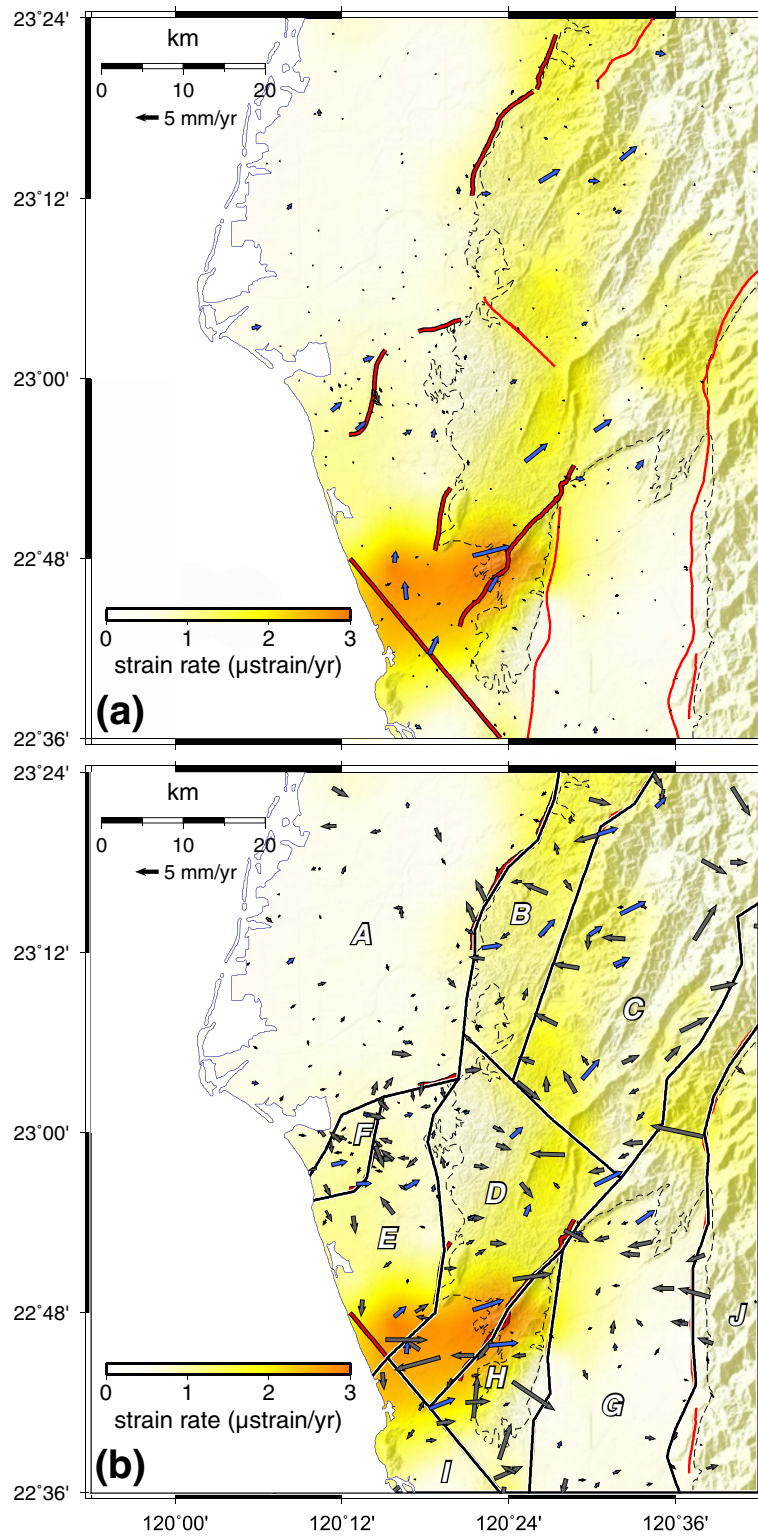


**Fig. 6** Distribution of velocity residuals in SW Taiwan. *Black vectors* are residuals of the horizontal velocities ( $RMS^{interior}$ ) derived from the 221 campaign-mode GPS stations. *Blue vectors* are the residual errors of horizontal velocities ( $RMS^{exterior}$ ) from 44 continuous GPS stations. *Red lines* are locations of active faults. *Thick red lines* are the active faults emphasized in this study. Colored map is the strain rate field derived from horizontal velocities. **a** Velocity residuals inferred from the Kriging method. **b** Velocity residuals inferred from the block model. *Black lines* denote the block boundaries

In this study, the observed coordinates of the 44 continuous GPS stations in the study area (Fig. 1) were compared with their corresponding transformed coordinates to analyze the accuracy of the coordinate transformation. The RMS was evaluated using Eq. 1 for the residuals in different epochs (Table 2 and Fig. 7). The RMS of the residuals quickly increased from  $\pm 7.8$  mm in 2004–2005 to  $\pm 19.1$  mm in 2004–2009. Based on these results, coordinate transformation is not an appropriate method for reducing the distortion caused by crustal deformation between different time epochs in a local area. The longer the time interval is, the greater the residuals of the coordinate transformation are. Moreover, the distribution of control points and surface deformation are the main limitations of coordinate transformation. In a local area, uniformly distributed control points and uniform surface deformation are essential for achieving a high-quality coordinate transformation. The 33 control points used in this study were not uniformly distributed (Fig. 7a). Therefore, coordinate transformation could not satisfactorily reduce the horizontal distortions in this study.

#### Precision of velocity models

In this study, the Kriging interpolation method and block model were used to establish the horizontal velocity model for SW Taiwan. The average residual  $\text{RMS}^{\text{interior}}$  of the Kriging method is considerably lower than that of the block model. Therefore, performance evaluations of the two methods were conducted to determine which is more suitable for establishing a surface horizontal velocity model for SW Taiwan.

First, the signals in surface deformation are composed of the tectonic block motion, coupling coefficients due to friction on the fault plane, seasonal variation, deep-seated landslide, volcanic activity, artificial groundwater withdrawal, and so on (e.g., Murray-Moraleda 2011). The temporal variations in the coordinate time series are stable from some of aforementioned mechanisms, such as the tectonic block motion and locking on the fault plane caused by tectonic loading. The first-order pattern of a horizontal velocity field generally represents tectonic movements. However, the temporal variation of the coordinate time series resulting from deep-seated landslide or groundwater pumping may not be stable (Fig. 8). Those mechanisms temporarily change the orientation of the velocity vector. Block model of velocity tend to consist of tectonic block motions and interseismic coupling on faults. In other words, modeling events caused by inelastic deformation, such as folding, deep-seated landslide, and artificial groundwater pumping, is difficult. By contrast, the Kriging interpolation method

attempts to minimize prediction errors, which are themselves estimated (Oliver and Webster 1990). Therefore, the performance of the Kriging method in minimizing residuals is superior to that of the block model.

Next, to evaluate the precision performance of the two methods, 44 continuous GPS stations observed from 2002 to 2010 in the study area were adopted for exterior checking (blue arrow lines in Figs. 1 and 6). The  $\text{RMS}^{\text{exterior}}$  values of the residual errors of horizontal velocities from 44 continuous GPS stations were calculated using Eq. 1. The  $\text{RMS}^{\text{exterior}}$  values of the Kriging method for the north and east components are  $\pm 1.9$  and  $\pm 2.2$  mm/year, respectively, and those of the block model are  $\pm 2.0$  and  $\pm 2.9$  mm/year, respectively (Fig. 6). The  $\text{RMS}^{\text{exterior}}$  of the two models is comparable in value and spatial distribution (Fig. 6). In addition, the  $\text{RMS}^{\text{interior}}$  and  $\text{RMS}^{\text{exterior}}$  of the block model are almost consistent. Compared with the Kriging method, the block model is a physical model and is constrained by geological parameters, such as the locations of faults, dips of faults, and sense of fault slips. Therefore, under a suitable geological constraint, the  $\text{RMS}^{\text{interior}}$  and  $\text{RMS}^{\text{exterior}}$  of the block model are consistent. However, for the Kriging method, favorable  $\text{RMS}^{\text{exterior}}$  values of  $\pm 1.9$  and  $\pm 2.2$  mm/year for the north and east components, respectively, are based on dense spatial coverage of the horizontal velocity field.

Although the Kriging method can easily establish a velocity model, a high station density (e.g., the approximately 5 km spacing in this study area) is required for providing a satisfactory spatial coverage condition for interpolation in SW Taiwan. In addition, a long data-acquisition duration is also required to minimize contamination from inelastic deformation or artificial sources. Conversely, constructing a block model of velocity is relatively difficult because more geological information is required to build the block boundaries and fault parameters (McCaffrey 2002). However, fewer observations are required in the tectonic block model because of the physical constraints originating from geological investigations.

Finally, according to the patterns in the  $\text{RMS}^{\text{exterior}}$  of the Kriging method and  $\text{RMS}^{\text{interior}}$  and  $\text{RMS}^{\text{exterior}}$  of the block model (Fig. 6), the distribution of residuals greater than 5 mm/year along blocks B, C, D, E, F, and H of the block model (Fig. 6b) generally corresponds to the high strain rate area derived from the horizontal velocity field, particularly for vectors in blocks D, E, F, and H (Fig. 6). Notably, orientations of some velocity vectors in blocks B and C, such as those of stations S336 and G126, are sub-perpendicular to the strikes of mountains (Fig. 4). Although there is no strong evidence proving that these vectors are contaminated by the deep-seated

**Table 2** RMS of the residuals of the observed and transformed coordinates of 44 continuous GPS stations in five periods (mm)

	2004 to 2005	2004 to 2006	2004 to 2007	2004 to 2008	2004 to 2009
RMS	±7.8	±10.8	±12.4	±15.9	±19.1

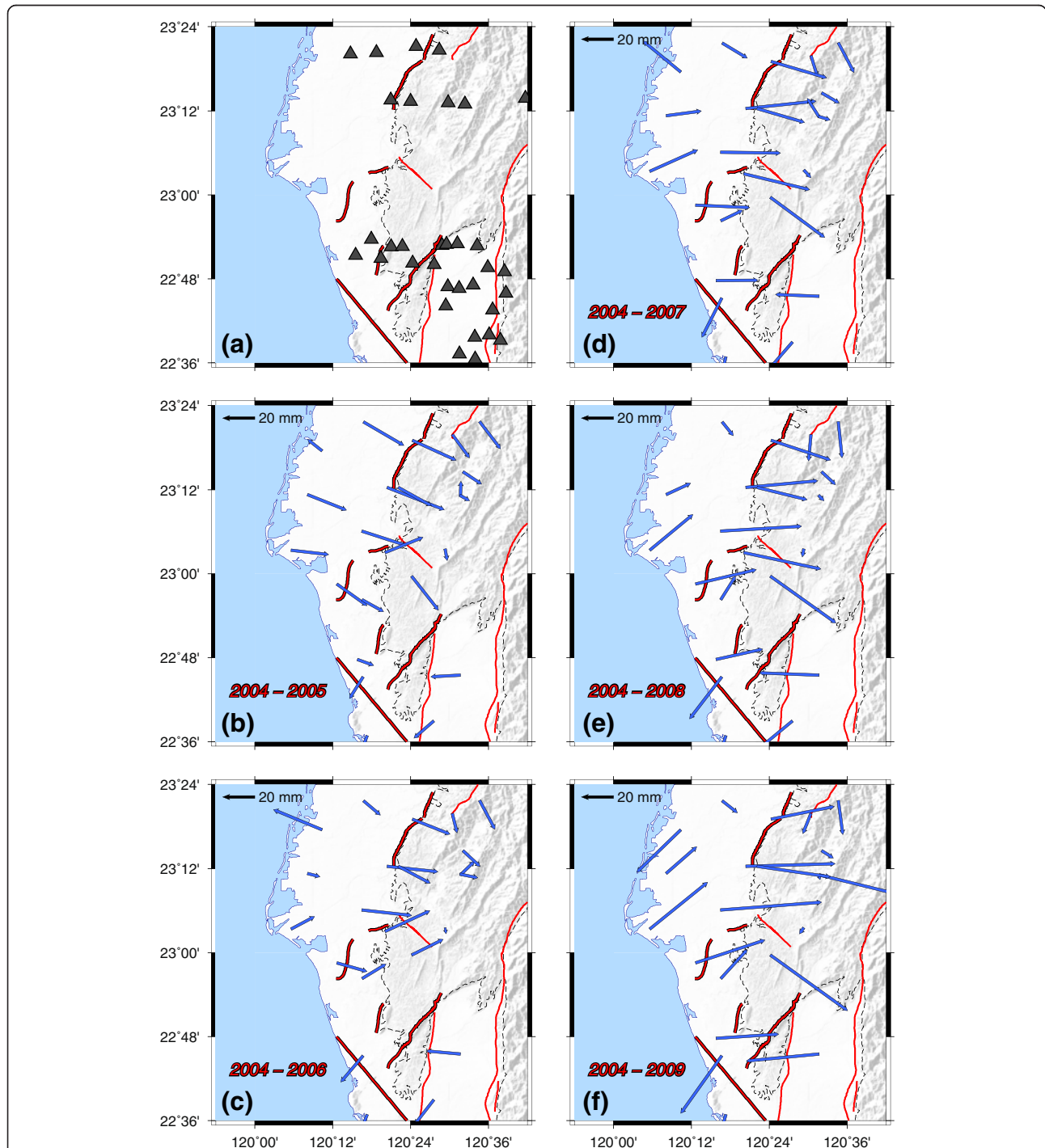


**Fig. 7** The coordinate residuals of the 44 continuous GPS stations in different epochs using the coordinate transformation. *Red lines* are locations of active faults. *Thick red lines* are the active faults emphasized in this study. **a** Distribution of 33 selected control points for the coordinate transformation. **b–f** The coordinate residuals in different epochs. *Blue vectors* are the residual errors of 44 continuous GPS stations

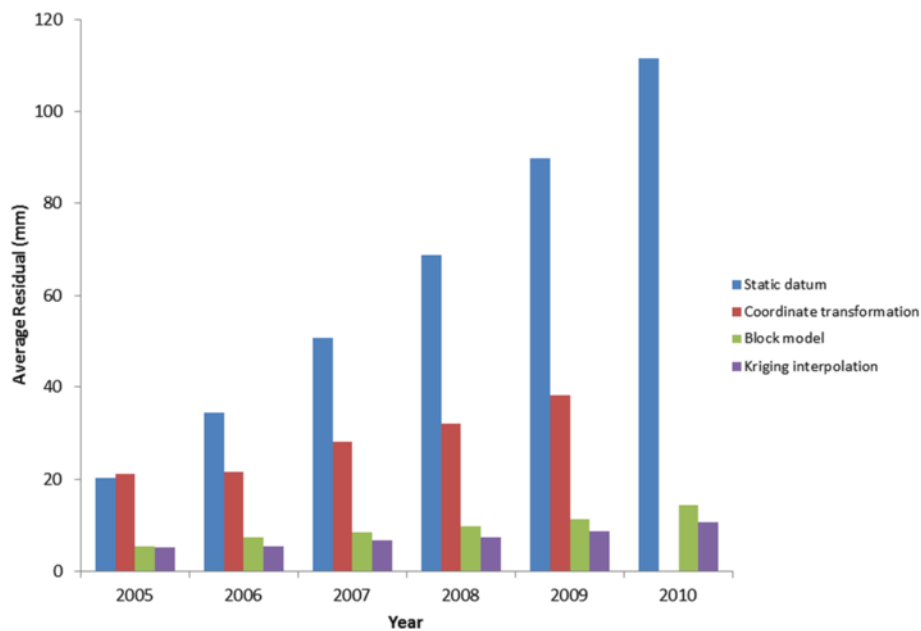


**Fig. 8** Temporal variation of the coordinate residuals of the 44 continuous GPS stations in different epochs using the static datum, coordinate transformation, block model, and Kriging interpolation method

landslide, the poor data fitting of the block model in blocks B and C and the orientations of these vectors sub-normal to the strikes of mountains may imply that deep-seated landslide disturbs the horizontal velocities. In addition, folding or mud diapir in a mudstone area, which acts as a non-recoverable, inelastic strain, is a crucial structural feature in blocks D, E, F, and H (Hsieh 1972; Lacombe et al. 1997, 2004; Pan 1968; Shih 1967) (Fig. 6). Therefore, modeling surface deformation caused by active folding or mud diapir in a mudstone area is difficult by using an elastic block model. In addition to the possibilities of deep-seated landslide and active fold or mud diapir in a mudstone area, these residuals may be attributable to poorly defined block boundaries or unclear fault parameters, because a detailed geological investigation is still required to clarify the present-day characteristics of active structures.

### Conclusions

A national geodetic datum is crucial in studying Earth science, establishing basic infrastructure, developing technology, and conducting academic analyses in a country. Therefore, to consider the tectonic effect in the Taiwan national geodetic datum, 221 campaign-mode GPS observations from 2002 to 2010 were employed to establish a surface horizontal velocity model for SW Taiwan by using the Kriging method and block model. According to exterior checking of the 44 continuous GPS stations in the study area, the averages of the residual errors ( $\text{RMS}^{\text{exterior}}$ ) obtained using the Kriging

method for the north and east components are  $\pm 1.9$  and  $\pm 2.2$  mm/year, respectively, and those obtained using the block model are  $\pm 2.0$  and  $\pm 2.9$  mm/year, respectively. Similar exterior checking results regarding the Kriging interpolation method and block model in SW Taiwan indicated a high station density and a relatively satisfactory station spatial coverage in the study area. However, the block model is more favorable than the Kriging method while lack of observation sites due to the consideration of characteristics of the geological structure.

Traditional coordinate transformation was used to compare with the coordinate precision of semi-dynamic datum. Comparing the Kriging method and block model revealed that the RMS of the residuals of the coordinate transformation rapidly increased from  $\pm 7.8$  in 2005 to  $\pm 19.1$  in 2009 (Fig. 8). Therefore, coordinate transformation is not an appropriate method for eliminating distortion over a long time in a deformed area.

In this study, only surface horizontal motions were considered to establish a horizontal velocity model for the semi-dynamic datum. The effects of coseismic and post-seismic deformation were not considered. Therefore, in the future, crustal deformation models should include the surface vertical velocity field, coseismic displacements, and postseismic deformation caused by major earthquakes.

### Abbreviations

TWD97: Taiwan Geodetic Datum 1997; GPS: Global Positioning System; ITRF94: International Terrestrial Reference Frame 1994; ITRF2008: International Terrestrial Reference Frame 2008; LCMF: Liuchia–Muchiliao fault system; HHAF: the Hsinhua fault; HCLF: the Houchiali fault; HKSF: the Hsiaokangshan

fault; CHNF: the Chishan fault; FTFZ: the Fengshan transfer fault zone; DEM: Digital Elevation Model; IGS: International GNSS Service; LSE: least squares estimation; RMS: root mean square.

#### Competing interests

The authors declare that they have no competing interests.

#### Authors' contributions

Both KEC and KHC initiated the study. KEC helped with the conceptual ideas, collected the data, and also helped write most of the article. KHC helped in the data calculated and analyses. Both authors contributed in interpreting the results and writing the paper as well. All authors read and approved the final manuscript.

#### Acknowledgements

We thank the Central Geological Survey for providing the campaign-mode GPS data. We thank the Central Weather Bureau, the Ministry of Interior, the National Land Surveying and Mapping Center, the Central Geological Survey, and the Institute of Earth Sciences, Academia Sinica for providing the continuous GPS data. Figures were generated using the Generic Mapping Tools (GMT), developed by Wessel and Smith (1991). This research was supported by Taiwan NSC grant NSC 101-2116-M-006-012-.

#### Author details

<sup>1</sup>Department of Geomatics, National Cheng Kung University, Tainan 70101, Taiwan. <sup>2</sup>Department of Real Estate and Built Environment, National Taipei University, New Taipei City 23741, Taiwan.

Received: 11 August 2015 Accepted: 15 December 2015

Published online: 30 December 2015

#### References

- Altamimi Z, Collilieux X, Métivier L (2011) ITRF2008: an improved solution of the international terrestrial reference frame. *J Geod* 85:457–473
- Beavan J, Blick G (2007) Limitations in the NZGD2000 deformation model. *Dyn Planet* 130:624–630
- Beavan J, Haines J (2001) Contemporary horizontal velocity and strain-rate fields of the Pacific-Australian plate boundary zone through New Zealand. *J Geophys Res* 106:741–770
- Bonilla MG (1977) Summary of Quaternary faulting and elevation changes in Taiwan. *Mem Geol Soc China* 2:43–56
- Bos AG, Spakman W, Nyst MCJ (2003) Surface deformation and tectonic setting of Taiwan inferred from a GPS velocity field. *J Geophys Res* 108:2458. doi:10.1029/2002JB002336
- Byrne T, Chan YC, Rau RJ, Lu CY, Lee YH, Wang YJ (2011) The arc-continent collision in Taiwan. doi:10.1007/978-3-540-88558-0\_8
- Chang HT (2004) Arbitrary affine transformation and their composition effects for two-dimensional fractal sets. *Image Vis Comput* 22(13):1117–1127
- Chang CP, Chang TY, Angelier J, Kao H, Lee JC, Yu SB (2003) Strain and stress field in Taiwan oblique convergent system: constraints from GPS observations and tectonic data. *Earth Planet Sci Lett* 214:115–127
- Chen B C (2005) A study on the southern part of Chishan fault. Dissertation, National Cheng Kung University
- Cheng SN, Yeh YT (1989) Catalog of the earthquakes in Taiwan from 1604 to 1988. Academia Sinica, Taipei
- Ching KE, Rau RJ, Lee JC, Hu JC (2007) Contemporary deformation of tectonic escape in SW Taiwan from GPS observations, 1995–2005. *Earth Planet Sci Lett* 262:601–619
- Ching K E, Johnson K M, Rau R J, Chuang R Y, Kuo L C, Leu P L (2011a) Inferred fault geometry and slip distribution of the 2010 Jiashian, Taiwan, earthquake is consistent with a thick-skinned deformation model. *Earth Planet Sci Lett* 301: 78–86
- Ching K E, Rau R J, Johnson K M, Lee J C, Hu J C (2011b) Present-day kinematics of active mountain building in Taiwan from GPS observations during 1995–2005. *J Geophys Res* 116 B09405. doi:10.1029/2010JB008058
- Chou JT (1971) A preliminary study of the stratigraphy and sedimentation of the mudstone formations in the Tainan area, southern Taiwan. *Petrol Geol Taiwan* 8:187–219
- Dach R, Hugentobler U, Fridez P, Meindl M (2007) Bernese GPS Software Version 5.0. University of Berne
- Deffontaines B, Lee JC, Angelier J, Carvalho J, Rudant JP (1994) New geomorphic data on the active Taiwan orogen: a multisource approach. *J Geophys Res* 99:20243–20266
- Deffontaines B, Lacombe O, Angelier J, Chu HT, Mouthereau F, Lee CT, Deramond J, Lee JF, Yu MS, Liew PM (1997) Quaternary transfer faulting in the Taiwan Foothills: evidence from a multisource approach. *Tectonophysics* 274:61–82
- Fruneau B, Pathier E, Raymond D, Deffontaines B, Lee CT, Wang HT, Angelier J, Rudant JP, Chang CP (2001) Uplift of Tainan foreland (SW Taiwan) revealed by SAR Interferometry. *Geophys Res Lett* 28:3071–3074
- Ghilani CD (2010) Adjustment computations: spatial data analysis. John Wiley & Sons, New Jersey
- Goovaerts P (1997) Geostatistics for Natural Resources Evaluation. Oxford University Press: 496
- Gourley J R, Lee YH, Ching KE (2012) Vertical fault mapping within the Gutingkeng Formation of southern Taiwan: implications for sub-aerial mud diapir tectonics. In: Abstract of the AGU Fall Meeting, San Francisco, Calif., 3–7 Dec 2012
- Grant DB, Blick GH (1998) A new geocentric datum for New Zealand (NZGD2000). *New Zealand Surveyor* 288:40–42
- Hsieh SH (1972) Subsurface geology and gravity anomalies of the Tainan and Chungchou structure of the coastal plain of southwestern Taiwan. *Petrol Geol Taiwan* 10:323–338
- Hsu TL, Chang HC (1979) Quaternary faulting in Taiwan. *Mem Geol Soc China* 3:155–165
- Hsu YJ, Yu SB, Simons M, Kuo LC, Chen HY (2009) Interseismic crustal deformation in the Taiwan plate boundary zone revealed by GPS observations, seismicity, and earthquake focal mechanisms. *Tectonophysics* 479:4–18
- Hu JC, Hou CS, Shen LC, Chan YC, Chen RF, Huang C, Rau RJ, Chen KH, Lin CW, Huang MH, Nien PF (2007) Fault activity and lateral extrusion inferred from velocity field revealed by GPS measurements in the Pingtung area of southwestern Taiwan. *J Asian Earth Sci* 31:287–302
- Huang ST, Yang KM, Hung JH, Wu JC, Ting HH, Mei WW, Hsu SH, Lee M (2004) Deformation front development at the northeast margin of the Tainan basin, Tainan-Kaohsiung area, Taiwan. *Mar Geophys Res* 25:139–156
- Huang MH, Hu JC, Hsieh CS, Ching KE, Rau RJ, Pathier E, Fruneau B, Deffontaines B (2006) A growing structure near the deformation front in SW Taiwan as deduced from SAR interferometry and geodetic observation. *Geophys Res Lett* 33:L12305. doi:10.1029/2005GL025613
- Huang MH, Hu JC, Ching KE, Rau RJ, Hsieh CS, Pathier E, Fruneau B, Deffontaines B (2009) Active deformation of Tainan tableland of southwestern Taiwan based on geodetic measurements and SAR interferometry. *Tectonophysics* 466:322–334
- Kuo HY, Wang CY, Chiu GT, Lee CY (1998) Houchiali Fault: an Active Fault? 7th Conference of Geophysics Society 429–437, Taiwan (in Chinese)
- Lacombe O, Angelier J, Chen HW, Deffontaines B, Chu HT, Rocher M (1997) Syndepositional tectonics and extension-compression relationships at the front of the Taiwan collision belt: a case study in the Pleistocene reefal limestones near Kaohsiung, SW Taiwan. *Tectonophysics* 274:83–96
- Lacombe O, Mouthereau F, Deffontaines B, Angelier J, Chu HT, Lee CT (1999) Geometry and Quaternary kinematics of fold-and-thrust units of southwestern Taiwan. *Tectonics* 18:1198–1223
- Lacombe O, Mouthereau F, Angelier J, Deffontaines B (2001) Structural, geodetic and seismological evidence for tectonic escape in SW Taiwan. *Tectonophysics* 333:323–345
- Lacombe O, Angelier J, Mouthereau F, Chu HT, Deffontaines B, Lee JC, Rocher M, Chen RF, Siame L (2004) The Liuchiu Hsu island offshore SW Taiwan: tectonic versus diapiric anticline development and comparisons with onshore structures. *C R Geoscience* 336:815–825
- Lee CT, Chen CT, Chi YM, Liao CW, Liao CF, Lin CC (2000) Engineering Investigation of Hsinhua Fault. National Central University 7 (in Chinese)
- Majdański M (2012) The structure of the crust in TESZ area by Kriging interpolation. *Acta Geophys* 60:59–75
- McCaffrey R (2002) Crustal block rotations and plate coupling, in Plate Boundary Zones. *Geodyn Ser* 30:101–122
- Miura H (2010) A study of travel time prediction using universal Kriging. *TOP* 18: 257–270
- MOI (2012) Report of Taiwan Geodetic Datum 1997 at 2010.0. Ministry of the Interior (MOI), Republic of China (Taiwan). <http://www.gps.moi.gov.tw/sscenter/>. Accessed 5 April 2012 (in Chinese)
- Mouthereau F, Deffontaines B, Lacombe O, Angelier J (2002) Variation along the strike of the Taiwan thrust belt, basement control on structural style, wedge geometry and kinematics. *Geol Soc Am* 358:31–53

- Murray-Moraleda J (2011) GPS: applications in crustal deformation monitoring. In: Meyers R (ed) *Extreme environmental events*, Springer, New York, pp 589–622
- Okada Y (1985) Surface deformation due to shear and tensile faults in a half-space. *Bull Seism Soc Am* 75:1135–1154
- Oliver MA, Webster R (1990) Kriging: a method of interpolation for geographical information systems. *Int J Geogr Inf Sci* 4:313–332
- Pan YS (1968) Interpretation aid seismic coordination of the Bouguer gravity anomalies obtained in southern Taiwan. *Petrol Geol Taiwan* 6:197–207
- Press WH, Flannery BP, Teukolsky SA, Vetterling WT (1989) *Numerical recipes*. U. K, Cambridge
- Roush JJ, Lingle CS, Guritz RM, Fatland DR, Voronina VA (2003) Surge-front propagation and velocities during the early-1993–95 surge of Bering Glacier, Alaska, U.S.A., from sequential SAR imagery. *Ann Glaciol* 36:37–44
- Samsonov S, Tiampo K (2006) Analytical optimization of a DInSAR and GPS dataset for derivation of three-dimensional surface motion. *IEEE Geosci Remote Sens Lett* 3:107–111
- Samsonov S, Tiampo K, Rundle J, Li Z (2007) Application of DInSAR-GPS optimization for derivation of fine-scale surface motion maps of Southern California. *IEEE Geosci Remote Sens Lett* 4:512–521
- Savage JC, Simpson RW (1997) Surface strain accumulation and the seismic moment tensor. *Bull Seism Soc Am* 87:1345–1353
- Shih TT (1967) A survey of the active mud volcanoes in Taiwan and a study of their types and the character of the mud. *Pet Geol Taiwan* 6:259–311
- Shyu JBH, Sieh K, Chen YG, Liu CS (2005) Neotectonic architecture of Taiwan and its implications for future large earthquakes. *J Geophys Res* 110, B08402. doi:10.1029/2004JB003251
- Sun SC (1971) Photogeologic study of the Hsinying-Chiayi coastal plain, Taiwan. *Petrol Geol Taiwan* 8:65–75
- Tanaka Y, Saita H, Sugawara J, Iwata K, Toyoda T, Hirai H, Kawaguchi T, Matsuzaka S (2007) Efficient maintenance of the Japanese geodetic datum 2000 using crustal deformation models—PatchJGD & semi-dynamic datum. *Bull Geogr Surv Inst* 54:49–59
- Tregoning P, Jackson R (1999) The need for dynamic datums. *Geomatics Research Australasia* 71:87–102
- van Dalen W, Doornenbal JC, Dortland S, Gunnink JL (2006) A comprehensive seismic velocity model for the Netherlands based on lithostratigraphic layers. *Netherlands J Geosci* 85–4:277–292
- Wackernagel H (2003) *Multivariate geostatistics: an introduction with applications*. Springer.
- Yu SB, Chen HY, Kuo LC (1997) Velocity field of GPS stations in the Taiwan area. *Tectonophysics* 274:41–59

**Submit your manuscript to a SpringerOpen<sup>®</sup> journal and benefit from:**

- Convenient online submission
- Rigorous peer review
- Immediate publication on acceptance
- Open access: articles freely available online
- High visibility within the field
- Retaining the copyright to your article

---

Submit your next manuscript at ► [springeropen.com](http://springeropen.com)

---